Petroleum Science 20 (2023) 1077–1086

Contents lists available at ScienceDirect

Petroleum Science

journal homepage: www.keaipublishing.com/en/journals/petroleum-science

Original Paper

# Assessing reservoir connectivity with pressure/rate surveillance data

G.F.J. Al-Khmaysawee [a], Z. Reza [b], C.S. Kabir [c, *]

[a] Missouri University of Sci. & Tech., Rolla, MO, USA
[b] University of Oklahoma, Norman, OK, USA
[c] Incendium Technologies, Round Rock, TX, USA

ARTICLE INFO

*Article history:*
Received 3 July 2022
Received in revised form
28 September 2022
Accepted 29 September 2022
Available online 9 October 2022

Edited by Yan-Hua Sun

*Keywords:*
Reservoir compartmentalization
Reciprocal-productivity index
Total material-balance time
Analysis of boundary-dominated flow period

ABSTRACT

Estimating reservoir connectivity is critical for assessing infill-drilling prospects and initiating fluid injection in enhanced oil recovery operations. Several methods have appeared in the literature over decades to meet these business needs, given that all tools, including seismic imaging, have limitations. Besides imaging, geochemical fingerprinting constitutes a powerful tool to gauge the compartmentalization question. However, real-time pressure/rate surveillance data allows assessing interwell connectivity vis-à-vis the overall drainage volume.

This study presents a simplified approach to using the reciprocal-productivity index (RPI) vs. the total-material-balance time ($\bar{t}_{TMB}$) plot. This tool exhibits the same slope for those wells in the same compartment beyond the start of the boundary-dominated flow (BDF) period. The wells showing different slopes imply that they are in separate drainage volumes. The early-time transient period remains muted to minimize confusion on this Cartesian plot. We validated the proposed tool's efficacy with 2D and 3D models with increased degrees of reservoir complexity, followed by the verification phase with four field examples. The use of other analytical tools complemented our findings.


## 1. Introduction

Methods have evolved over decades to learn about reservoir connectivity. Also, assessing the drainage volume associated with each well is an item of interest for field development strategy. In other words, understanding interwell connectivity should precede planning of any fluid injection and infill drilling whenever the project economics becomes the prime driver.

Geochemical fingerprinting of reservoir fluids is one of the robust tools that has been in use for over five decades. This technology largely owes to the evolving nature of the analysis techniques, as chronicled by Kamber (2009). Interestingly, Larter et al. (1997) characterized this technology as a link between reservoir geology and engineering, given that it ascertains reservoir continuity. Among many are basin-specific studies (Westrich et al., 1999) and field-specific (Kaufman et al., 2000, 2002; Elshahawi et al., 2008, 2010; Asemani et al., 2021) abound in the literature.

Among various simple analytical tools involving pressure and rate, the $p/q$ plot (Kabir and Izgec, 2009) and the primary capacitance-resistance model or PCRM (Izgec and Kabir, 2011) provide considerable insights into reservoir connectivity or lack thereof. In this context, multiwell deconvolution also plays an important role; the studies of Levitan (2007), Onur et al. (2011), Cumming et al. (2014), among others, are cases in point. We note that the conventional pulse or interference tests have become uncommon in field operations, given the intrinsic operational requirements for a pair of wells of interest. In fluid injection, tracer tests (Refunjol and Lake, 1999) and, more recently, capacitance-resistance modeling or CRM can shed light on the injector-producer connectivity. Some of these related studies include those of Albertoni and Lake (2003), Sayarpour et al. (2009), Izgec and Kabir (2010), Kaviani and Valko (2010), Kaviani et al. (2012), Parekh and Kabir (2013), de Holanda et al. (2018), and Kumar et al. (2020).

From an earth science perspective, many definitions for reservoir connectivity exist, as discussed by Chen (2013), Snedden et al. (2007), Vrolijk (2005), among others. How reservoir connectivity is measured and modeled can be operator specific. Some define it based on the number of wells in the reservoir; others prefer connectivity indices that rely on criteria that gauge how complex the

* Corresponding author.
*E-mail address:* shah@incencendiumtech.com (C.S. Kabir).

https://doi.org/10.1016/j.petsci.2022.09.037

**Nomenclature**

| | |
|---|---|
| $c_k$ | Total system compressibility, 1/psi |
| $I_{RP}$ | Reciprocal productivity index, psi·d/STB |
| $k$ | Formation permeability, mD |
| $N$ | Reservoir drainage volume associated with a well, STB |
| $p_i$ | Initial reservoir pressure, psia |
| $p_{wf}$ | Flowing bottomhole pressure, psia |
| $q$ | Fluid flow rate, STB/d |
| $Q$ | Cumulative production, STB |
| $t$ | Producing time, d |
| $\bar{t}_{TMB}$ | Total material-balance time for multiple wells, d |

*Abbreviations*

| | |
|---|---|
| RPI | Reciprocal-productivity index |
| BDF | Boundary-dominated flow |
| MBT | Material-balance time |
| TMB | Total material balance |
| CRMP | Capacitance-resistance model for producer |
| PCRM | Primary capacitance-resistance model |
| RTA | Rate transient analysis |

*Subscripts*

| | |
|---|---|
| $k$ | Well number |
| RP | Reciprocal-productivity |
| TMB | Total material balance |

reservoir is to develop or invest. Ideally, the simplest definition of reservoir connectivity needs anchoring on fundamental reservoir property that measures the degree of communication between the wells that penetrate the reservoir.

There are two types of connectivity: static and dynamic, and many definitions and methods exist to evaluate them. Static connectivity describes the native state, which depends on the structure, stratigraphy, heterogeneity, and other reservoir properties before production start-up, as Snedden et al. (2007) described. The evaluation depends on the geological data, whereas many parameters used to assess it relies on the method used in the assessment (Kaviani et al., 2012). Dynamic connectivity describes the state of the reservoir during production, depending on time-dependent reservoir characterizations, such as pressure and saturation (Snedden et al., 2007). Engineering data involves interference and pulse testing, as Kaviani et al. (2012) used. Since CRM's introduction in 2003 has taken its root in industrial applications for assessing injector/producer connectivity. In the Wang et al. (2020) study, several signal processing techniques support CRM findings by resolving the injector-producer distance and well interference effect despite the multiwell reservoir complexities.

This study uses both production rate and pressure data to evaluate interwell connectivity. Given the various options and the required time and expertise for data interpretation, this article proposes using a simple analytical reciprocal-productivity index or RPI tool. This tool requires plotting RPI ($I_{RP}$) vs. the total-material-balance time ($\bar{t}_{TMB}$), involving the wells of interest to gauge their connectivity. Wells draining from the same connected pore volume will overlay and exhibit a positive slope on this Cartesian plot. One can use this tool whenever production rate and the attendant bottomhole pressure data become available, such as those in offshore settings. For gas or gas/condensate reservoirs, conversion of wellhead pressure to downhole conditions is feasible in both onshore and offshore operations. Three synthetic cases involving various degrees of reservoir compartments verified the proposed approach, followed by four field examples that aided the validation phase.

## 2. Methodology

In a rate-transient analysis for a single well, we use the productivity index or PI, its integral, and its derivative as a function of the material-balance time or MBT. The use of three responses helps diagnose the overall signature of the BDF period in the Blasingame plot. In contrast, the log-log plot uses the RPI vs. MBT and the RPI integral derivative to diagnose the BDF period's presence with the unit-slope response.

As shown by Kabir and Izgec (2009) in Eq. (B-9), we can represent the reciprocal productivity index or RPI ($I_{RP}$) as follows for a multiwell system:

$$I_{RP} = \frac{p_i - p_{wf,k}(t)}{q_k(t)} = \frac{1}{NC_k}\bar{t}_{TMB} + f(t) \tag{1}$$

Note that the variable $f(t)$ becomes constant during the BDF period. Therefore, the same drainage volume wells will exhibit the same positive slope on the $I_{RP}$ vs. $\bar{t}_{TMB}$ plot. These slopes overlay during the BDF period when sufficient interwell connectivity or high-conductive flow paths exist; otherwise, they will have parallel slopes. In Eq. (1), the left side shows the $I_{RP}$ for individual wells. In contrast, $\bar{t}_{TMB}$ represents the total material-balance time for the interacting wells within a drainage volume containing $N$ stock-tank barrels. We note that Marhaendrajana and Blasingame (2001) provided the underlying foundational work.

Let us point out that the previous study in 2009 used the $p/q$ diagnosis to examine the three flow regimes, involving the transient period with a negative slope, followed by the constant-rate or tubing-limited flow period with a vertical response or zero slopes. Finally, the BDF period emerged with a positive slope. In contrast to the conventional $p/q$ approach, this study uses Eq. (1) to show the value proposition of this approach in various reservoir settings. In this context, three synthetic cases validated our solution approach, and four field examples verified our diagnostic procedure to assess reservoir compartmentalization. We also used other analytical tools to seek corroboration of the RPI approach. In addition, our findings suggested that the linear plot provides more clarity than the log-log approach for identifying the compartments in a multiwell setting, given that this approach premises on the BDF period.

As discussed above and verified and validated in subsequent sections with synthetic and field examples, we think $I_{RP}$ vs. $\bar{t}_{TMB}$ is a powerful subsurface diagnostic tool to infer reservoir communication and, in some instances, "reservoir compartmentalization." As a result, this section proposes a robust measure of well interference using RPI and MBT. We first cast Eq. (1) into the following form, where we employ a volume of influence based on $N$ that is a function of $\bar{t}_{TMB}$ for an individual well as:

$$N_k = N_k(\bar{t}_{TMB}) \tag{2}$$

Note that we can consider $N_k(\bar{t}_{TMB})$ as a portion of the oil-in-place (or the reservoir volume) that feeds the production of well $k$, which may change in time in the event of interference from other adjacent wells. This outcome results in a smaller or larger volume of influence that feeds the producer. Another extreme subsurface scenario can appear when a fault breach occurs, resulting in the producer's enlarged reservoir volume. In other words, these subsurface events can shrink or extend the reservoir boundary for the well in question. Let us refer to these subsurface events as "interference events." With this premise, we propose the following:

$$I_{RP}(t) = \frac{p_i - p_{wf,k}(t)}{q_k(t)} = \frac{1}{N_k(\bar{t}_{TMB})\, c_k}\bar{t}_{TMB} + f(t) \quad (3)$$

When the current boundary dominates the flow; that is, $t \to \infty$, $f(t) = f$, we have

$$I_{RP}(t) = \frac{1}{N_k(\bar{t}_{TMB})\, c_k}\bar{t}_{TMB} + f \quad (4)$$

In RPI - MBT space, the slope $m_{I_{RP}-\bar{t}_{TMB}}$ represents the following:

$$m_{I_{RP}-\bar{t}_{TMB}} = \frac{1}{N_k(\bar{t}_{TMB})\, c_k} \quad (5)$$

Thus,

$$N_k(\bar{t}_{TMB}) = \frac{1}{m_{I_{RP}-\bar{t}_{TMB}}\, c_k} \quad (6)$$

When an interference event occurs, say at $\bar{t}_{TMB1}$, the slope of $I_{RP}$ vs. $\bar{t}_{TMB}$ will change from $m_{I_{RP}-\bar{t}_{TMB}}$ to $m_{I_{RP}-\bar{t}_{TMB1}}$. A steeper slope will amount to shrinking the in-place volume feeding the producer, implying an adjacent well or wells are draining from the influence region of the well in question. On the other hand, if the slope decreases, the influence volume of the well in question enlarges. In this case, this well is draining a more significant part of the reservoir. Of course, these interpretations assume that the total system compressibility remains constant. In other words, these interference events do not affect the reservoir's fluid properties or storage capacity.

Therefore, we can characterize the interference events by the following expressions:

$$N_k(\bar{t}_{TMB1}) < N_k(\bar{t}_{TMB0}), \text{if } m_{I_{RP}-\bar{t}_{TMB}} 1 > m_{I_{RP}-\bar{t}_{TMB}}, \quad (7)$$

and

$$N_k(\bar{t}_{TMB1}) > N_k(\bar{t}_{TMB0}), \text{if } m_{I_{RP}-\bar{t}_{TMB}} 1 < m_{I_{RP}-\bar{t}_{TMB}}, \quad (8)$$

## 3. Verification and validation of the RPI tool

This section first verified the proposed reservoir compartmentalization approach with three case studies. Both homogeneous and heterogeneous porous media provided the platform for verification by generating data with numerical models for both single-phase and multiphase flow. Following this approach, field data from four diverse geologic settings helped validate the efficacy of the proposed methodology. We used other tools like PCRM, RTA, CRMP, and $p/q$ diagnosis while soliciting corroboration.

### 3.1. Model verification with synthetic reservoir systems

**Case-1.** Three-compartment homogeneous reservoir

We first started with a simple homogeneous baffled reservoir system with 100 mD permeability and 44% porosity to test the proposed tool's usefulness. Fig. 1a presents a homogeneous oil reservoir involving four wells in a three-compartment system. The corresponding RPI plot in Fig. 1b shows the depletion behavior in three compartments with different slopes. The overlying slopes in Wells 1 and 2 indicate that they are in one high-conductive flow compartment. In contrast, the steepest slope for Well 4, followed by that in Well 3, implies smaller drainage volumes than Wells 1 and 2. Yes, the steeper slope indicates smaller pore volume in a relative sense. Overall, the RPI conveys connectivity and the relative compartment volume in a multiwell setting. Table A-1 presents calculation steps for two of the four wells' plotting variables, $I_{RP}$ and $\bar{t}_{TMB}$. We included all four wells in these steps while calculating the total cumulative production, leading to the estimation of $\bar{t}_{TMB}$.

We then explored the efficacy of the primary-capacitance-resistance model (PCRM) tool in ascertaining this interwell connectivity or lack thereof. The conventional rate-transient analysis (RTA) helped estimate the in-place volume with PCRM for each well. However, as Fig. 2 displays, discerning compartmentalization

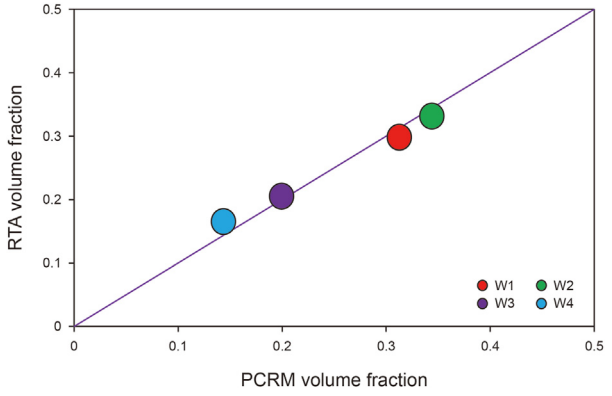


**Fig. 2.** Comparing RTA and PCRM pore volumes associated with each well does not suggest definitive compartmentalization.

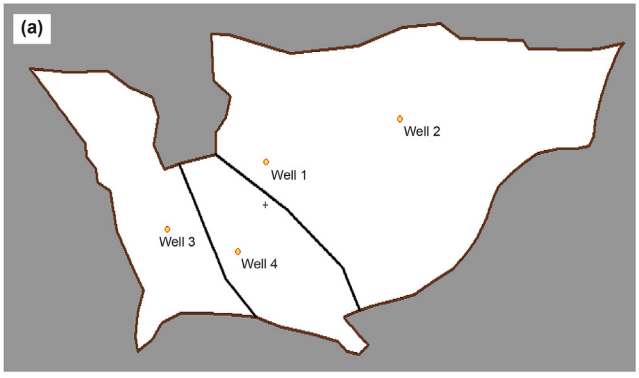


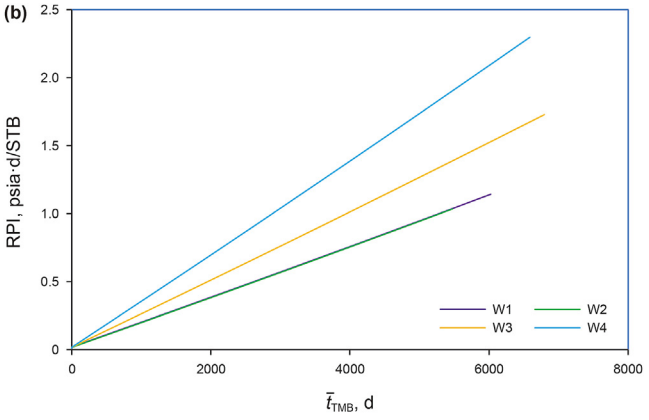


**Fig. 1.** Field map for four wells with impenetrable barriers (**a**), the resultant RPI responses indicate well connectivity or lack thereof (**b**).

appears to be within a margin of error in this case. Note that the volume fraction in Fig. 2 implies each well's volume to the total reservoir volume. Given the large area that Wells 1 and 2 occupy, their volume fractions are higher than Wells 3 and 4, located in smaller compartments. Of course, the sum of these fractional volumes must add up to one.

**Case-2.** Lateral heterogeneity in a communicating system

Starting with the Case-1 model, we introduced lateral heterogeneity by creating a simple increment of permeability from left to right in each colored region, as shown in Fig. 3a. Region 12 has 50 mD, Region 11 has 55 mD, and Region 10 has 60 mD. After that, permeability increased by 10 mD from Region 10 to Region 1. The creation of a simple lateral heterogeneity underpinned this idea.

As expected, Fig. 3b shows the parallel RPI responses according to a region's permeability. Well 2, in the highest permeability area, exhibits the lowest RPI response, whereas Well 3 shows the opposite outcome. In between, Wells 1 and 4 responses appear. Permeability variation in each well's region, in this case, governs this overall outcome. The parallel nature of these RPI responses represents the variability of rock properties, such as permeability for this case, in this otherwise contiguous system. As expected, RPI increased with a decrease in the region's permeability. Fig. 4 displays that the two independent tools, PCRM and RTA, generated the exact solutions for all four wells, and this methodology reaffirms the lack of compartmentalization.

**Case-3.** 3D heterogeneous reservoir system

To better understand interwell connectivity in a realistic reservoir setting, we generated results for a 3D heterogeneous reservoir involving multiphase flow during the primary production phase. Fig. 5 presents the field map with three vertical and three horizontal producers. Table 1 presents the grid cell properties, and Fig. 6a displays the porosity distribution, whereas Fig. 6b shows the associated permeability.

We assigned ten years of production period for each well. Fig. 7a shows the initial pressure map, whereas Fig. 7b presents the distributed pressure after ten years of production. Nonuniform change in color reaffirms the impact of heterogeneity on production performance during primary depletion.

Fig. 8, displaying the RPI plot, tells us about the connectivity between Wells HW1 and HW2 and Wells HW3 and VW1. In contrast, Wells VW2 and VW3 exhibit isolation with decreasing-PI or increasing-RPI performance. These observations juxtapose very well with input and performance data shown in Figs. 5–7.

Given the scale compression in Fig. 8, let us amplify the well interference between Wells HW1 and HW2. Fig. 9 shows the slope

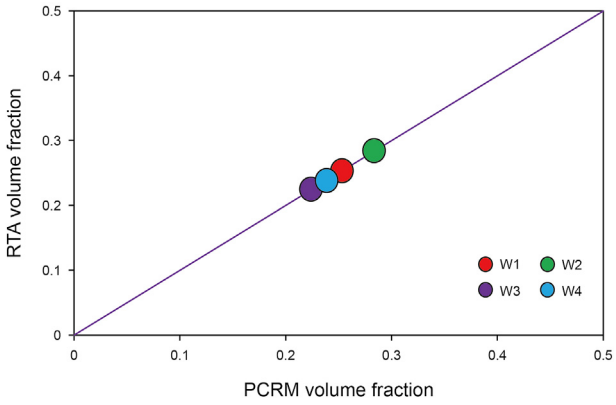


**Fig. 4.** RTA and PCRM reaffirmed reservoir connectivity by the pore volumes associated with each well.

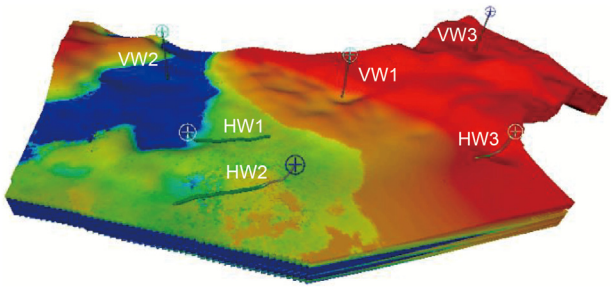


**Fig. 5.** The field map identifies the well locations involving three vertical and three horizontal producers.

change of the $I_{RP} - \bar{t}_{TMB}$ plot for the two wells. The slope for Well HW2 decreases, suggesting this well experiences a larger drainage volume after the interference event. In contrast, the slope for Well HW1 increases, which implies the drainage volume of Well HW1 gets intercepted by the other well, Well HW2. Inarguably, the proposed method can objectively detect and quantify well interference events, leading to enhanced reservoir management practices strategizing.

The steeper slope in Fig. 8 implies a rapid decline in the productivity index, given a smaller pore volume than a shallower slope. As Fig. 8 shows, when the slopes overlay (Wells VW1 and HW3, Wells HW1 and HW2), the degree of interference is intense, meaning they are in the same compartment.

Note that the intercept implies the time to reach the boundary-dominated flow (BDF) period. In other words, the higher intercept

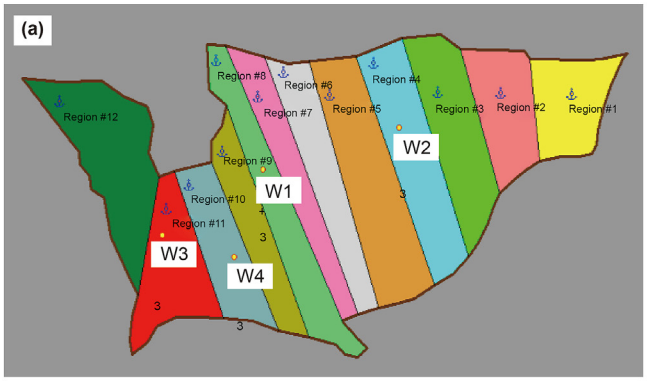


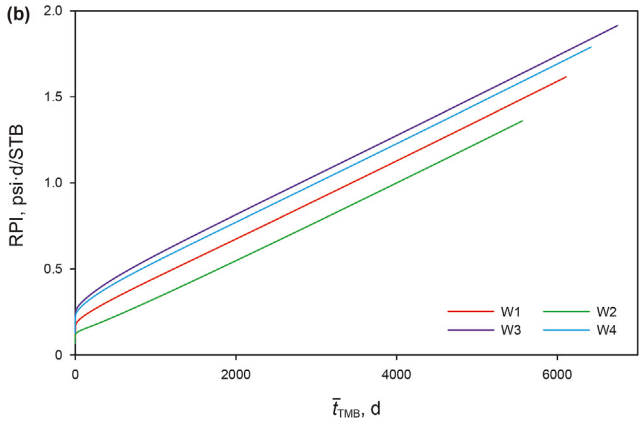


**Fig. 3.** Field map for four wells with lateral heterogeneity (**a**), the parallel RPI signatures indicate well connectivity (**b**).

**Table 1**
Model's grid cell properties.

| Number of zones | | Number of *X* grid cells | | | Number of *Y* grid cells | | | Number of layers |
|---|---|---|---|---|---|---|---|---|
| 4 | | 216 | | | 312 | | | 119 |
| Zone | Porosity | | | | Permeability, mD | | | |
| | Min. | Mean | SD | Max. | Min. | Mean | SD | Max. |
| Zone 1 | 1.E−04 | 0.082 | 0.08 | 0.4 | 0.2 | 13.9 | 14.6 | 99.1 |
| Zone 2 | 1.E−04 | 0.055 | 0.047 | 0.4 | 0.1 | 2.3 | 1.7 | 10.0 |
| Zone 3 | 1.E−04 | 0.054 | 0.047 | 0.4 | 1.4 | 9.3 | 4.2 | 24.9 |
| Zone 4 | 1.E−04 | 0.044 | 0.025 | 0.32 | 0.4 | 12.3 | 11.6 | 99.3 |

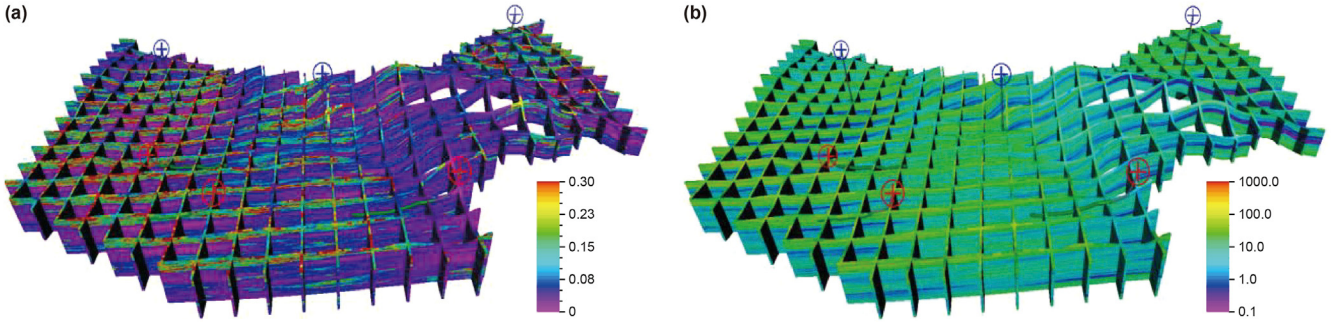


**Fig. 6.** The 3D grids show the variability of porosity (**a**) and permeability (**b**) involving four zones.

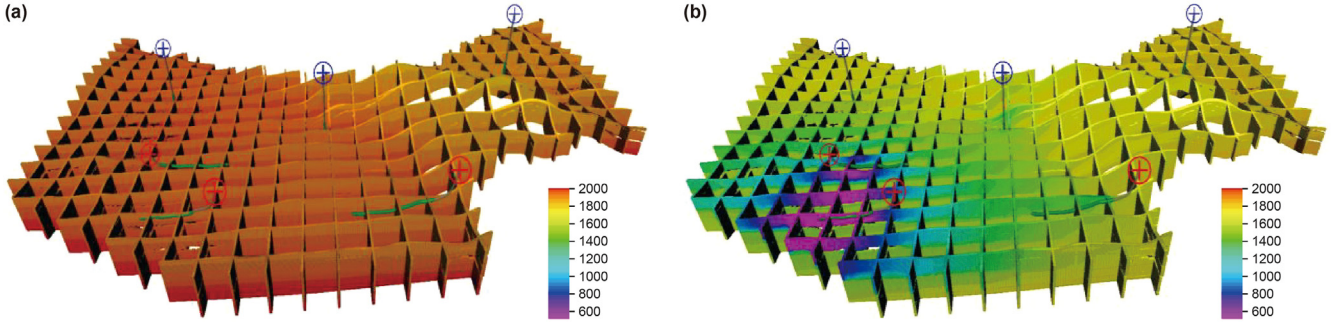


**Fig. 7.** Uniformity of pressure trend appears at the initial condition (**a**), and differences occur at the end of 10 years of production (**b**) involving four zones.

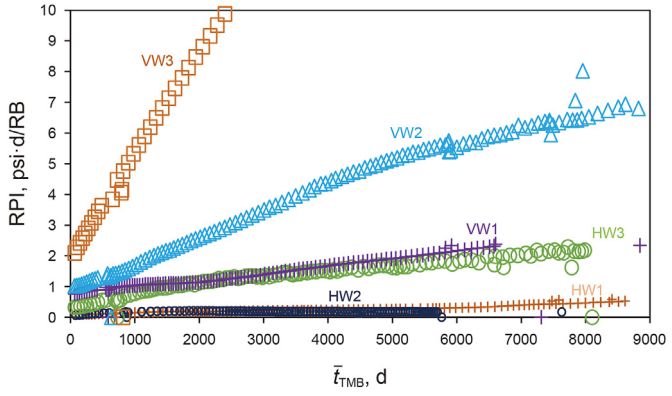


**Fig. 8.** RPI plot shows connectivity between Wells HW1 and HW2, Wells HW3 and VW1, whereas Wells VW2 and VW3 are isolated.

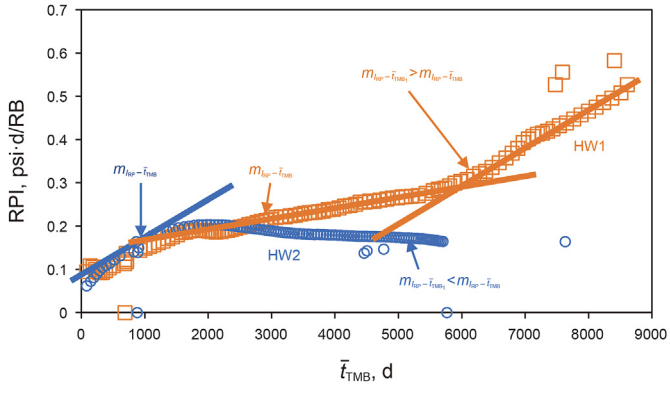


**Fig. 9.** Amplification of the RPI plot shows connectivity between Wells HW1 and HW2 at early times, but divergence occurs at late times.

indicates a low-permeability region associated with a given well, as the higher RPI value or the low-productivity index suggests. Nevertheless, the steeper slope means a higher depletion rate in each situation. For instance, Well VW3 in Fig. 8 exhibits the steepest slope, implying the lowest associated pore volume relative to five other wells. In this context, the larger green domain, as shown in

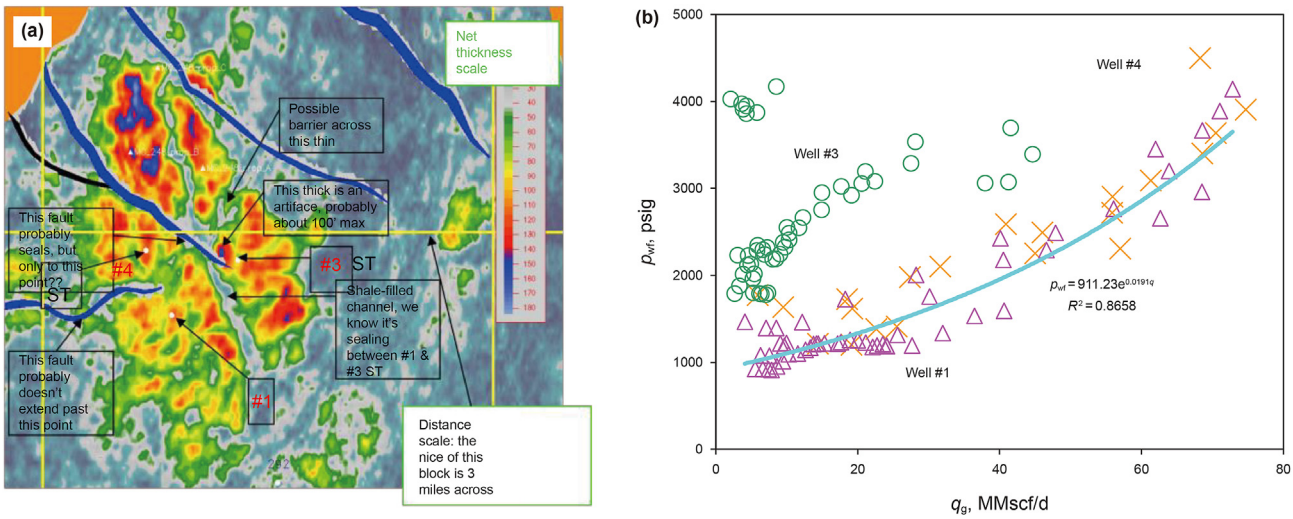


**Fig. 10.** The seismic map shows possible compartmentalization (**a**), the *p*/*q* plot shows connectivity between Wells 1 and 4, but not Well 3 (**b**).

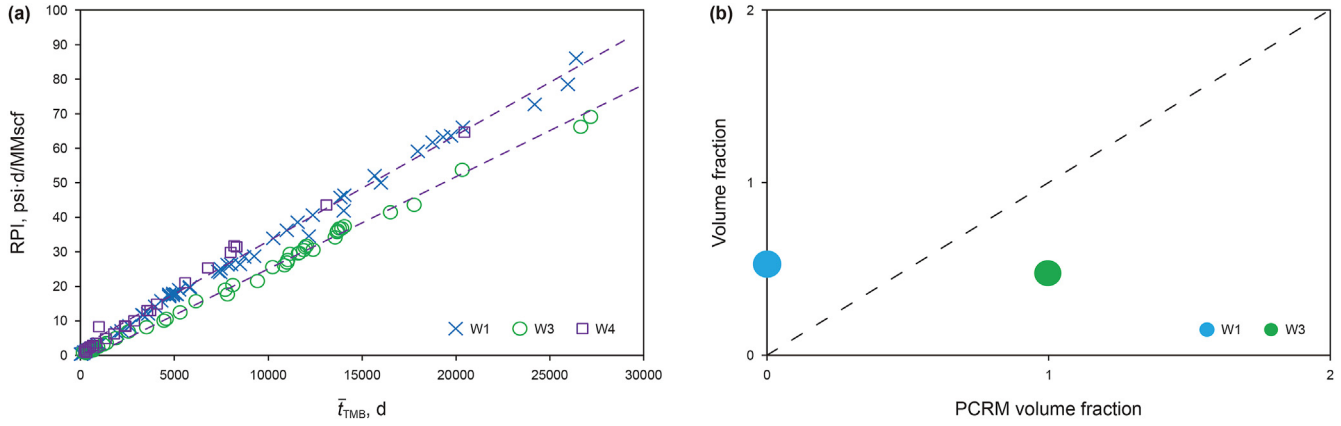


**Fig. 11.** RPI plot shows Well 3 is in a separate compartment relative to Wells 1 and 4 (**a**); PCRM analysis also supports this outcome (**b**).

Fig. 5, means that both Wells HW1 and HW2 experience energy support despite having higher productivity indices.

### 3.2. Model validation with field reservoir systems

This section presents four field examples to validate the RPI methodology proposed in this study. Except for the Volve field, whose data has been made available in the public domain, the other three examples appeared earlier in other studies.

#### 3.2.1. FE-1: Gulf of Mexico example

This field example appeared in an earlier study by Kabir and Izgec (2009). Fig. 10a shows the seismic map indicating possible isolation of Well 3 in another compartment, as supported by the *p*/*q* plot in Fig. 10b. Fig. 11a, showing the RPI plot, corroborates the lesson learned earlier; Wells 1 and 4 are in the same compartment, whereas Well 3 is in a separate fault block. The PCRM approach also supports the notion that Well 3 is in a different fault block, as Fig. 11b shows.

The proposed method is relevant during the boundary-dominated flow, which can be diagnosed with the unit-slope response on a log-log plot of RPI vs. material-balance time. This outcome is simply because depletion from a given drainage volume provides the necessary information for ascertaining the time-dependent depletion period. Yes, this approach is unlike an interference test, wherein one well undergoes variable rate changes to convey the signal to another shut-in well to gauge the communication between the two. Given the practical difficulty of generating strong signals, meaning high-rate fluctuations, and well-shut-in, decades-long practice suggests its minimal use. However, as shown in Fig. 11b, using primary-CRM can also corroborate what the RPI method can deliver, as Fig. 11a demonstrates.

#### 3.2.2. FE-2: Volve field, Norwegian North Sea

In this Volve field example, we show the relative performance of four wells to keep the message simple for the dataset that appeared in the public domain. Fig. 12a shows the grid map with well locations with possible compartments, whereas Fig. 12b displays the water saturation map at the initial condition. Fig. 13 displays the RPI profiles for four wells. Only Wells F–11B and F-14 exhibit parallel slopes, thereby suggesting communication. Given their steeper slopes, Wells F-12 and F-15D offer smaller pore volumes than the other two. Overall, three compartments appeared by considering just four wells in this system.

#### 3.2.3. FE-3: Valhall field, North Sea

This field case reaffirms the same point as observed earlier. The reservoir heterogeneity can offer various degrees of

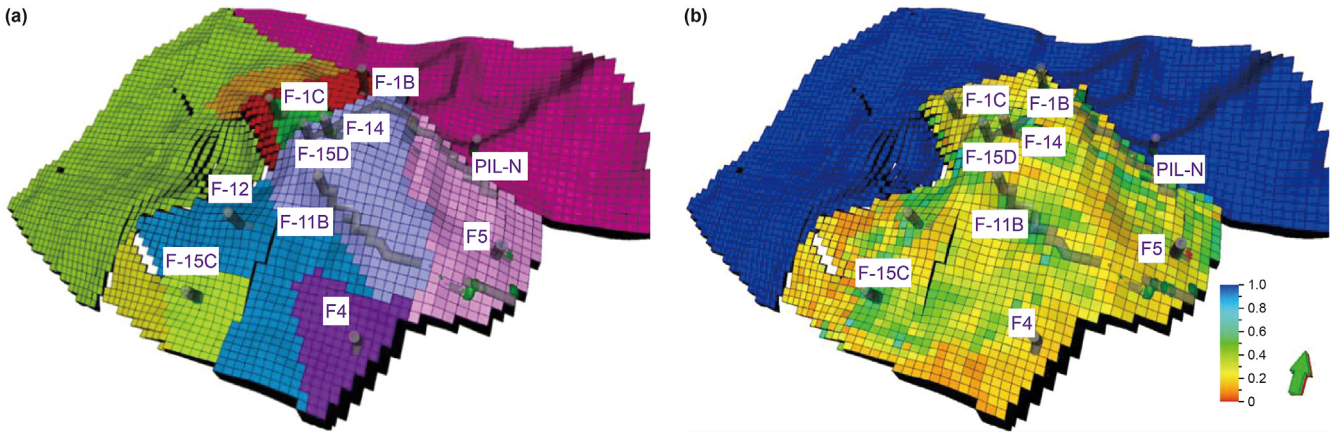


**Fig. 12.** The grid map for 3D numerical model for the Volve field shows many compartments (**a**), and variable water saturation at the initial condition (**b**).

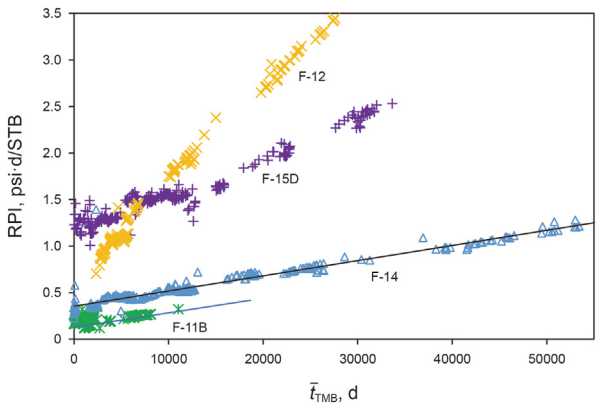


**Fig. 13.** Well connectivity appears for Wells F–11B and F-14 given their parallel slopes but not for the two other wells.

compartmentalization despite the wells' proximity. The details of this chalk field's performance analysis appear in the Kabir et al. (2016) article. Fig. 14a displays the field map in this field's crest. Even though Wells F03 and A12 appear very close in this chalk reservoir, they lay in separate compartments, as Fig. 14b shows. We note that those parallel lines for the A-12 producer relate to data quality, so we need to focus on the general trend. The early-time negative slopes for Well A-1 imply good pressure support from the G-22 injector, as learned from the CRMP results earlier (Kabir et al., 2016). This energy source keeps the RPI very low relative to Wells F-3 and A-12.

The earlier CRMP study results (2016) showed that about 80% of the G-22 injection supported the A1 producer and 17% for the A-5 producer. This vital communication between Wells G-22 and A-1 produced the near-horizontal low-RPI value, as shown in Fig. 14b. However, despite the proximity, the G-22 injector did not communicate with the A-12 and F-3 producers. These outcomes emphasize the complexity of the compartmentalization question in most reservoirs.

### 3.2.4. FE-4: Oil Field, UK North Sea

As discussed in a study by Kabir and Boundy (2011) involving various analytical tools and numerical modeling, this field provides further evidence of reservoir complexity regarding well connectivity, despite natural fractures. The seismic map in Fig. 15 suggests that Well A05 is in a separate compartment, which Fig. 16a reaffirms while contrasting the RPI performance with Well A9. In this context, Fig. 16b provides further evidence of different slopes, except Wells A9 and A1, as they appear to be in the same compartment.

As expected, all field production data contain noise. A large fraction of this noise arises due to the near-horizontal response in

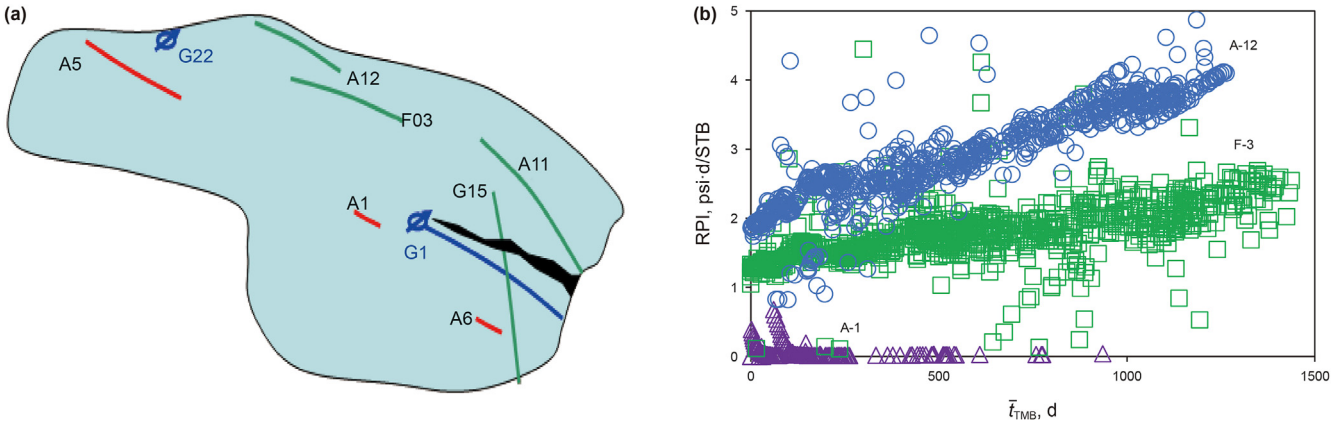


**Fig. 14.** The Valhall field map at the crest (**a**); RPI plot suggests that Wells A12 and F03 belong to different compartments (**b**).

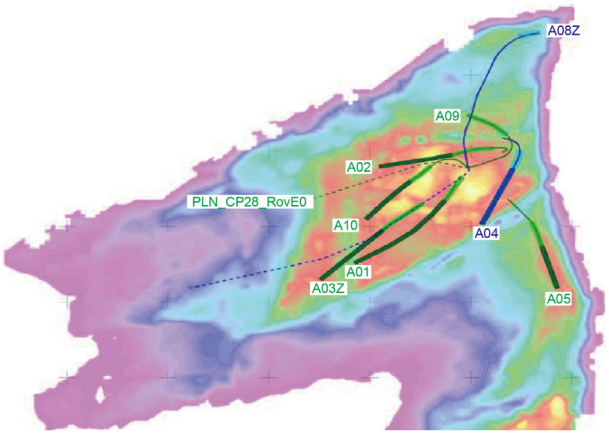


**Fig. 15.** The seismic map for the field.

the transient period. Despite that apparent obstacle, Fig. 16a, displaying the results of Wells A5 and A9, clearly indicates that they do not communicate over a long production period. In contrast, only Wells A1 and A9 appear to communicate, as the parallel slopes in Fig. 16b display.

## 4. Discussion

This study demonstrated a simplified RPI (reciprocal-productivity index plot) tool approach to seek interwell connectivity. As expected, each method requires specific data and interpretation tools. For example, at least two buildup tests over a broad timespan are necessary for the multiwell deconvolution solution approach to ascertain connectivity. In this context, the RPI approach, as espoused here, requires only the production rates and the associated pressures for generating the needed plot over time. In our view, this simplicity becomes the fundamental value proposition even with the multiphase flow.

As expected, the quality of interwell connectivity may change during the total production period due to changes in a well's PI. Generally, the PI change is associated with energy support, stimulation, operational issues, artificial lift, and solids precipitation, among others; Figs. 9 and 13 convey this message. Our current approach is qualitative. Estimating interwell connectivity by way of permeability will require a separate investigation. Note that the proposed method is invaluable for assessing producers' conversion into injectors and drilling injection wells. Ineffectiveness of waterfloods in the North Sea, as shown in field examples 2, 3, and 4, are cases in point. In other words, if we had this connectivity information in the project's early life, then the waterfloods' management could have been very different.

All analytical tools generally use the basic assumption of constant compressibility. With an increase in system compressibility, we expect a higher value for the Arps' *b*-factor. As a result, the PI and recovery factor would improve, resulting in a decline in RPI. Conversely, a decrease in total system compressibility would increase the RPI trend.

Despite the advent of 4D seismic imaging, real-time rate/pressure surveillance data can reveal interwell connectivity. This interwell connectivity or lack thereof early in a field's production life helps design and manage secondary and tertiary recovery projects. In addition, prospect evaluation of infill opportunities in gas fields in wastewater disposal and $CO_2$ sequestration projects also make value-added propositions. The proposed methodology becomes contextual in new field developments, especially offshore operations, where well costs largely dictate project economics. However, we note that when the downhole pressure gauges become dysfunctional after a few years of production in deepwater wells, a significant obstacle appears for real-time data gathering.

Djuraev et al. (2017), in their review article, discussed the pros and cons of various multidisciplinary tools for understanding reservoir performance. Given the strengths and limitations of a given methodology, they emphasized the simultaneous use of multiple devices for the overall sense of reservoir performance, leading to sound business decisions. These recommendations align well with our approach, wherein the proposed RPI method presents another independent way to show the interwell connectivity without requiring additional measuring devices or tests.

## 5. Conclusions

(1) The RPI vs. the total-MB time plot for multiple wells provides various clues about reservoir continuity vis-à-vis conductivity of the fluid-flow path. Here are the principal lessons learned:

(a) Differences in line slopes suggest different reservoir compartments, regardless of the physical proximity of wells.

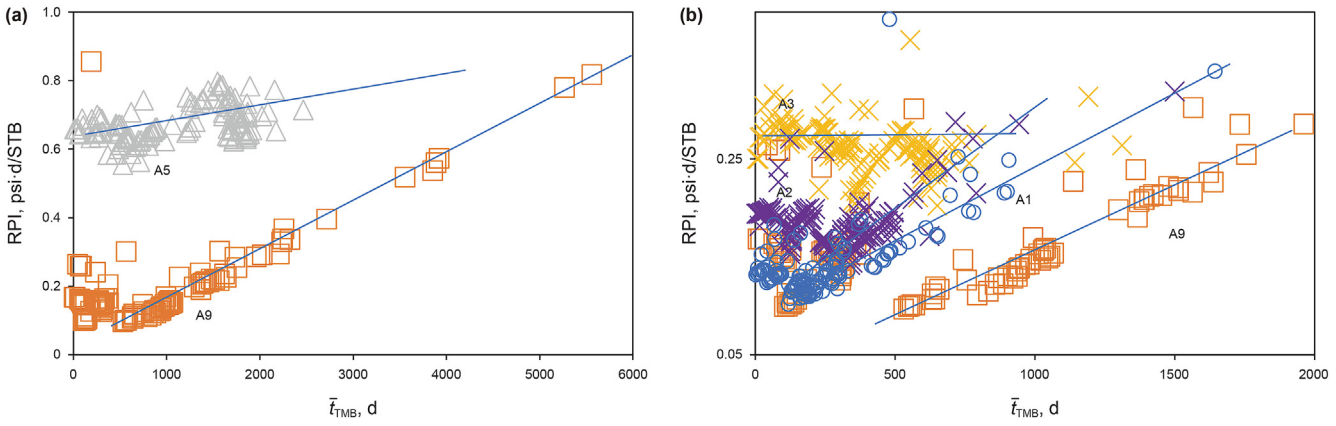


**Fig. 16.** The RPI plot suggests that Well A5 is separated from Well A9 (**a**); diversity of slopes appear in other wells, although communication exists between Wells A1 and A9 (**b**).

(b) The overlying slope suggests the same compartment with high conductivity.
(c) The separation with a parallel slope suggests the same compartment. However, the degree of separation signifies decreased lateral reservoir conductivity; the Volve field example is a case in point.
(d) Evolving nature of well interference becomes transparent, and its quantification becomes feasible, leading to realistic real-time reservoir management.

(2) Both PCRM and CRMP aided understanding of interwell connectivity, or lack thereof, thereby providing independent corroboration of the proposed RPI tool. Similarly, the $p/q$ plot also offered the necessary supporting evidence for the FE-1.

## Ethics & disclosures

We declare that the content resulted from an independent investigation and did not present it at any conference. We have no financial or non-financial information to disclose.

## Funding

We did not receive any funding for conducting this study.

## Declaration of competing interest

We have no conflicts of interest.

## Appendix A. Sample calculations for two wells in Case-1

**Table A-1**
The table shows stepwise calculations involving two of the four wells in Case-1.

| Time, d | $p_{wf}$, psia | | $I_{RP}$, psi·d/STB | | $Q^*$, STB | $\bar{t}_{TMB}$, d | |
|---|---|---|---|---|---|---|---|
| | Well 1 | Well 2 | Well 1 | Well 2 | | Well 1 | Well 2 |
| 0 | 3000 | 3000 | | | | | |
| 0.00 | 2886.76 | 2913.30 | 0.10 | 0.07 | 18.90 | 0.02 | 0.02 |
| 10.00 | 2770.90 | 2830.07 | 0.20 | 0.14 | 45160.54 | 39.54 | 36.16 |
| 20.00 | 2753.12 | 2819.67 | 0.22 | 0.14 | 90268.81 | 79.10 | 72.31 |
| 30.00 | 2737.93 | 2810.90 | 0.23 | 0.15 | 135349.63 | 118.67 | 108.46 |
| 60.00 | 2698.24 | 2786.43 | 0.26 | 0.17 | 270447.48 | 237.49 | 216.94 |
| 80.00 | 2674.21 | 2769.94 | 0.29 | 0.18 | 360402.38 | 316.79 | 289.28 |
| 90.00 | 2662.64 | 2761.55 | 0.30 | 0.19 | 405348.54 | 356.47 | 325.47 |
| 100.00 | 2651.28 | 2753.05 | 0.31 | 0.20 | 450274.40 | 396.15 | 361.66 |
| 150.00 | 2596.91 | 2709.15 | 0.36 | 0.23 | 674608.99 | 594.82 | 542.81 |
| 200.00 | 2545.05 | 2663.53 | 0.40 | 0.27 | 898470.26 | 793.85 | 724.25 |
| 300.00 | 2444.58 | 2569.46 | 0.49 | 0.35 | 1344825.78 | 1193.01 | 1088.14 |
| 400.00 | 2345.72 | 2473.47 | 0.58 | 0.43 | 1789399.54 | 1593.68 | 1453.42 |
| 500.00 | 2247.25 | 2376.50 | 0.67 | 0.51 | 2232214.86 | 1995.91 | 1820.14 |
| 600.00 | 2148.84 | 2278.97 | 0.76 | 0.59 | 2673284.28 | 2399.72 | 2188.32 |
| 700.00 | 2050.47 | 2181.10 | 0.86 | 0.67 | 3112617.56 | 2805.10 | 2557.95 |
| 800.00 | 1952.04 | 2083.03 | 0.95 | 0.76 | 3550222.51 | 3212.10 | 2929.02 |
| 900.00 | 1853.61 | 1984.83 | 1.04 | 0.84 | 3986106.42 | 3620.70 | 3301.58 |
| 1000.00 | 1755.13 | 1886.52 | 1.14 | 0.93 | 4420276.15 | 4030.90 | 3675.64 |
| 1100.00 | 1656.67 | 1788.14 | 1.23 | 1.01 | 4852738.59 | 4442.76 | 4051.14 |
| 1200.00 | 1558.17 | 1689.72 | 1.33 | 1.10 | 5283500.02 | 4856.21 | 4428.16 |
| 1300.00 | 1459.67 | 1591.28 | 1.42 | 1.19 | 5712567.41 | 5271.30 | 4806.64 |
| 1400.00 | 1361.14 | 1492.81 | 1.52 | 1.27 | 6139947.03 | 5688.06 | 5186.63 |
| 1500.00 | 1262.60 | 1394.31 | 1.62 | 1.36 | 6565645.49 | 6106.43 | 5568.13 |

*Note*: *Q represents all four wells.

## References

Albertoni, A., Lake, L.W., 2003. Inferring interwell connectivity only from well rate fluctuations in waterfloods. SPE Reservoir Eval. Eng. 6 (1), 6–16. https://doi.org/10.2118/83381-PA.
Asemani, M., Rabbani, A.R., Sarafdokht, H., 2021. Implementation of an integrated geochemical approach using polar and nonpolar components of crude oil for reservoir continuity assessment: verification with reservoir-engineering evidences. SPE J. 26 (5), 3237–3254. https://doi.org/10.2118/205388-PA.
Chen, J., 2013. Deepwater reservoir compartmentalization: causes, impacts on production, and methods of identification. Offshore Technol. Conf. https://doi.org/10.4043/23951-MS.
Cumming, J.A., Wooff, D.A., Whittle, T., Gringarten, A.C., 2014. Multiwell deconvolution. SPE Reservoir Eval. Eng. 17 (4), 457–465. https://doi.org/10.2118/166458-PA.
de Holanda, R.W., Gildin, E., Jensen, J.L., Lake, L.W., Kabir, C.S., 2018. A state-of-the-art literature review on capacitance resistance models for reservoir characterization and performance forecasting. Energies 11 (12), 3368. https://doi.org/10.3390/en11123368.
Djuraev, U., Jufar, S.R., Vasant, P., 2017. A review on conceptual and practical oil and gas reservoir monitoring methods. J. Petrol. Sci. Eng. 152 (2017), 586–601. https://doi.org/10.1016/j.petrol.2017.01.038.
Elshahawi, H., Venktramanan, L., McKinney, D., et al., 2008. Combining continuous fluid typing, wireline formation testers, and geochemical measurements for an improved understanding of reservoir architecture. SPE Res. Eng. Eval. 11 (1), 27–40. https://doi.org/10.2118/100740-PA.
Elshahawi, H., Mullins, O., Hows, M., et al., 2010. Reservoir fluid analysis as a proxy for connectivity in deepwater reservoirs. Petrophysics 51 (2), 75–88.
Izgec, O., Kabir, C.S., 2011. Quantifying reservoir connectivity, in-place volumes, and drainage-area pressures during primary depletion. J. Petrol. Sci. Eng. 81 (2012), 7–17. https://doi.org/10.1016/j.petrol.2011.12.015.
Izgec, O., Kabir, C.S., 2010. Quantifying nonuniform aquifer strength at individual wells. SPE Reservoir Eval. Eng. 13 (2), 296–305. https://doi.org/10.2118/120850-PA.
Kabir, C.S., Izgec, B., 2009. Diagnosis of reservoir compartmentalization from measured pressure/rate data during primary production. J. Petrol. Sci. Eng. 69 (3–4), 271–282. https://doi.org/10.1016/j.petrol.2009.09.007.
Kabir, C.S., Boundy, F., 2011. Analytical tools aid understanding of history-matching effort in a fractured reservoir. J. Petrol. Sci. Eng. 78 (2), 274–282. https://doi.org/10.1016/j.petrol.2011.05.018.
Kabir, C.S., Haftbaradaran, R., Asghari, R., Sastre, J.P., 2016. Understanding variable well performance in a chalk reservoir. SPE Reservoir Eval. Eng. 19 (1), 83–94. https://doi.org/10.2118/175436-PA.
Kamber, B.S., 2009. Geochemical fingerprinting: 40 years of analytical development

and real world applications. App. Geochemistry 24 (6), 1074–1086. https://doi.org/10.1016/j.apgeochem.2009.02.012.
Kaufman, R.L., Kabir, C.S., Abdul-Rahman, B., et al., 2000. Characterizing the Greater Burgan field with geochemical and other field data. SPE Reservoir Eval. Eng. 3 (2), 118–126. https://doi.org/10.2118/62516-PA.
Kaufman, R.L., Dashti, H., Kabir, C.S., et al., 2002. Characterizing the greater burgan field: use of geochemistry and oil fingerprinting. SPE Reservoir Eval. Eng. 5 (3), 190–196. https://doi.org/10.2118/78129-PA.
Kaviani, D., Jensen, J.L., Lake, L.W., 2012. Estimation of interwell connectivity in the case of unmeasured fluctuating bottomhole pressures. J. Petrol. Sci. Eng. 90–91 (1), 79–95. https://doi.org/10.1016/j.petrol.2012.04.008.
Kaviani, D., Valko, P.P., 2010. Inferring interwell connectivity using multiwell productivity index (MPI). J. Petrol. Sci. Eng. (1–2), 48–58. https://doi.org/10.1016/j.petrol.2010.05.006, 48–58.
Kumar, A., Seth, P., Shrivastava, K., et al., 2020. Integrated analysis of tracer and pressure-interference tests to identify well interference. SPE J. 25 (4), 1623–1635. https://doi.org/10.2118/201233-PA.
Larter, S.R., Aplin, A.C., Corbett, P.W.M., et al., 1997. Reservoir geochemistry: A link between reservoir geology and engineering? SPE Reservoir Eng. 12 (1), 12–17. https://doi.org/10.2118/28849-PA.
Levitan, M.M., 2007. Deconvolution of multiwell test data. SPE J. 12 (4), 420–428. https://doi.org/10.2118/102484-PA.
Marhaendrajana, T., Blasingame, T.A., 2001. Decline curve analysis using type curves–Evaluation of well performance behavior in a multiwell reservoir system. SPE Ann. Techn. Conf. Exhib. https://doi.org/10.2118/71517-MS.
Onur, M., Ayan, C., Kuchuk, F.J., 2011. Pressure-pressure deconvolution analysis of multiwell-Interference and interval-pressure-transient tests. SPE Reservoir Eval. Eng. 14 (6), 652–662. https://doi.org/10.2118/149567-PA.
Parekh, B., Kabir, C.S., 2013. A case study of improved understanding of reservoir connectivity in an evolving waterflood with surveillance data. J. Petrol. Sci. Tech. 102 (2013), 1–9. https://doi.org/10.1016/j.petrol.2013.01.004.
Refunjol, B.T., Lake, L.W., 1999. Reservoir characterization based on tracer response and rank analysis of production and injection rates. In: Schatzinger, R., Jordan, J. (Eds.), Reservoir Characterization-Recent Advances. Chap 15, 209–218. AAPG Memoir 71.
Sayarpour, M., Kabir, C.S., Lake, L.W., 2009. Field applications of capacitance-resistance models in waterfloods. SPE Reservoir Eval. Eng. 12 (6), 853–864. https://doi.org/10.2118/114983-PA.
Snedden, J.W., Vrolijk, P., Sumpter, L., Sweet, M.L., Barnes, K.R., White, E., Farrell, M.E., 2007. Reservoir connectivity: definitions, strategies, and applications. SPE Int. Petrol. Technol. Conf. https://doi.org/10.2523/IPTC-11375-MS.
Vrolijk, P., 2005. Reservoir connectivity analysis–Defining reservoir connections, and plumbing. SPE Middle East Oil Gas Show Conf. https://doi.org/10.2118/93577-MS.
Wang, Y., Kabir, C.S., Reza, Z., 2020. Deciphering well connectivity with diagnostic signal processing techniques. J. Petrol. Sci. Tech. 185 (Feb. 2020), 106610. https://doi.org/10.1016/j.petrol.2019.106610.
Westrich, J.T., Fuex, A.M., O'Neal, P.M., Halpem, H.I., 1999. Evaluating reservoir architecture in the Northern Gulf of Mexico with oil and gas chemistry. SPE Reservoir Eval. Eng. 2 (6), 514–519. https://doi.org/10.2118/59518-PA.